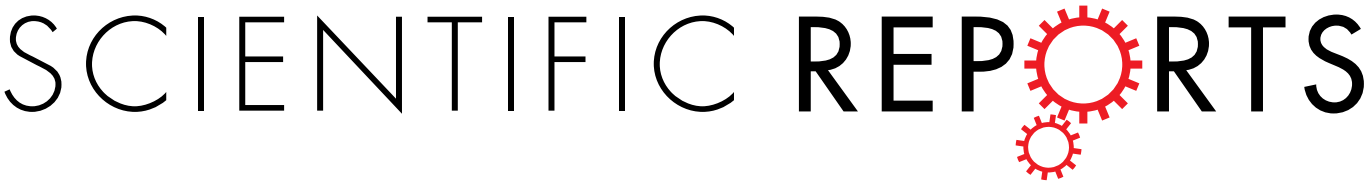

OPEN

Single-electron charge sensing in self-assembled quantum dots

Haruki Kiyama[1], Alexander Korsch[2], Naomi Nagai[3], Yasushi Kanai[1], Kazuhiko Matsumoto[1], Kazuhiko Hirakawa[3] & Akira Oiwa[1,4]

Received: 13 March 2018
Accepted: 14 August 2018
Published online: 18 September 2018

Measuring single-electron charge is one of the most fundamental quantum technologies. Charge sensing, which is an ingredient for the measurement of single spins or single photons, has been already developed for semiconductor gate-defined quantum dots, leading to intensive studies on the physics and the applications of single-electron charge, single-electron spin and photon–electron quantum interface. However, the technology has not yet been realized for self-assembled quantum dots despite their fascinating transport phenomena and outstanding optical functionalities. In this paper, we report charge sensing experiments in self-assembled quantum dots. We choose two adjacent dots, and fabricate source and drain electrodes on each dot, in which either dot works as a charge sensor for the other target dot. The sensor dot current significantly changes when the number of electrons in the target dot changes by one, demonstrating single-electron charge sensing. We have also demonstrated real-time detection of single-electron tunnelling events. This charge sensing technique will be an important step towards combining efficient electrical readout of single-electron with intriguing quantum transport physics or advanced optical and photonic technologies developed for self-assembled quantum dots.

Self-assembled quantum dots (QDs) have been a fascinating platform for the investigation of microscopic quantum physics and applications to nanoelectronics, spintronics and photonics. In InAs QD-based single-electron transistors[1], a variety of quantum transport experiments have been reported, including electrical control of the spin–orbit interaction[2] and g-factor[3,4], Josephson junction[5,6], spin valve[7,8] and terahertz spectroscopy[9]. In quantum information processing, the coupling between photons and InAs QDs offers key technologies, such as a single-photon source[10], single-spin manipulation[11] and entanglement between spins and photons[12,13]. Moreover, site-selective growth techniques are being developed[14,15], which are indispensable for constructing large-scale quantum devices comprising a number of dots.

For further developments of the potential abilities of self-assembled QDs, a charge sensing technique, which has greatly contributed to the development of gate-defined QDs towards spin-based quantum information processing[16], is strongly needed to be realized in the self-assembled QDs. Charge sensing has been realized by using a quantum point contact[17] or a single electron transistor[18] fabricated near the dots as a sensor. The conductance through the sensor is sensitive to the electrostatic environment at certain gate-voltage conditions. Because the sensor is placed close to the dot, the single-electron charging in the dot significantly changes the sensor conductance, enabling single-electron charge sensing. This technique works even if dot conductance is too small to measure, enabling detection of single-electron tunnelling events in real-time[18–20]. In addition, this real-time charge sensing allows for measurement of other physical quantities by converting them into electron charge: single-photon detection has been demonstrated by detecting single photo-excited electrons[21,22], and the readout of single-electron spin has been implemented by detecting spin-dependent tunnelling events[23–26]. Moreover, a few works on charge sensing have been reported for vertical QDs[27], carbon nanotube QDs[28] and nanowire QDs[29–31] by placing a sensor near a QD or by connecting a sensor and a QD with a floating gate. However, this has not yet been achieved for self-assembled QDs. Realizing charge sensing in a single-electron transistor based on a self-assembled QD may be challenging because the metal electrodes directly contacting the QD may effectively screen the single-electron charge in the QD[6].

[1]The Institute of Scientific and Industrial Research, Osaka University, 8-1 Mihogaoka, Ibaraki, Osaka, 567-0047, Japan. [2]Lehrstuhl für Angewandte Festkörperphysik, Ruhr-Universität Bochum, Universitätsstraße 150, Gebäude NB, D-44780, Bochum, Germany. [3]Institute of Industrial Science, The University of Tokyo, 4-6-1 Komaba, Meguro, Tokyo, 153-8505, Japan. [4]Center for Spintronics Research Network, Graduate School of Engineering Science, Osaka University, 1-3 Machikaneyama, Toyonaka, Osaka, 560-0043, Japan. Correspondence and requests for materials should be addressed to H.K. (email: kiyama@sanken.osaka-u.ac.jp)

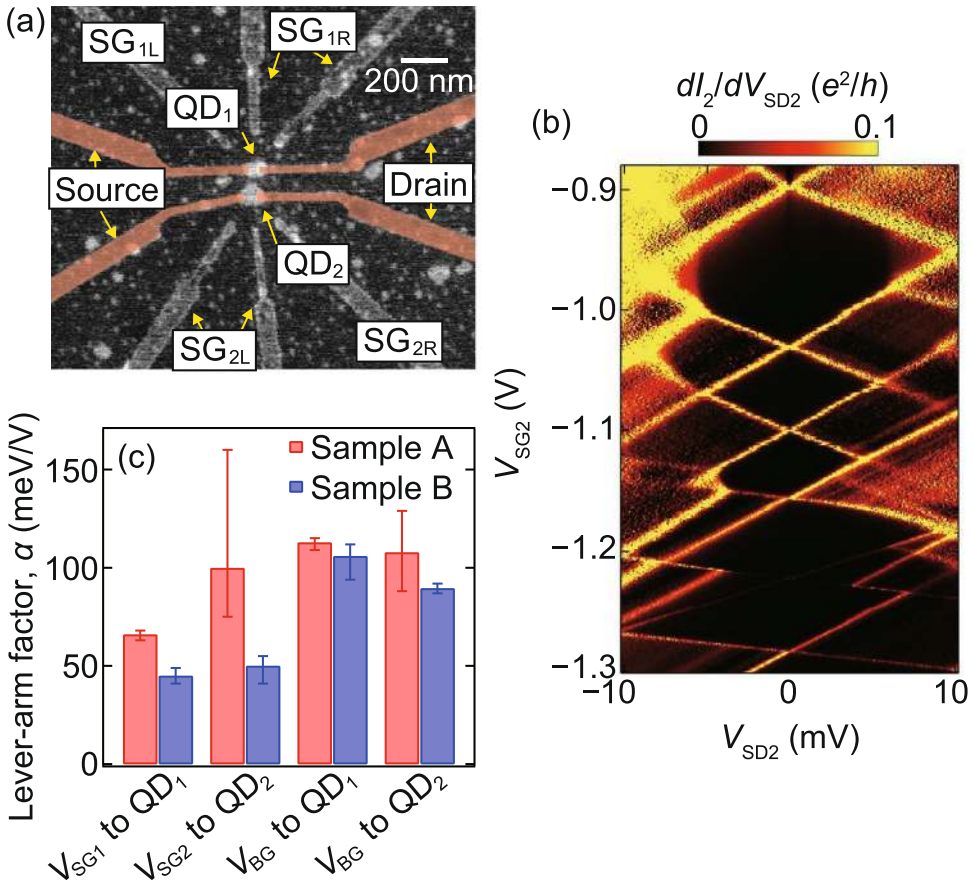

Figure 1. (**a**) Scanning electron micrograph of a device similar to the measured device. (**b**) The differential conductance of QD_2, dI_2/dV_{SD2}, in sample A as a function of V_{SD2} and V_{SG2} at $V_{BG} = 0$ V. (**c**) Lever-arm factor α of the side gates and the back gates for samples A and B.

In this work, we report single-electron charge sensing experiments in InAs self-assembled QDs by using another adjacent QD as a sensor. Metal electrodes contacting the QDs are made narrow for reducing the screening effect. The capacitive coupling between the two QDs is large enough to show the distinct change in the dot current induced by the single-electron charging in the adjacent dot. We also demonstrate charge sensing in real-time at the dot-reservoir resonance having the tunnel rate lower than the measurement bandwidth.

Results

Device. Two samples, A and B, studied in this work consist of two uncapped self-assembled InAs QDs, each contacted by a pair of Ti/Au (10/20 nm) electrodes as source and drain [see Fig. 1(a)]. The two QDs have a diameter and height of approximately 100 nm and 20 nm, respectively, which are suitable for stable single-electron transistor devices[1–9,32,33]. These dots are separated by approximately 150 nm from centre-to-centre. The source-drain electrode has a nanogap separation of approximately 50 nm and a width of approximately 50 nm. The latter is intentionally made narrow compared to the devices used in preceding studies[1–9,32,33], in order to reduce the screening effect[6] and hence enhance the charge sensitivity of the dots. Ti/Au electrodes surrounding the dots and a degenerately Si-doped GaAs layer buried 300 nm below the surface are used as local side gates and a global back gate, respectively, to control the electrostatic potential of the dots. For sample A, the $20 \times 20\ \mu$m region around the dots is covered by a 50-nm-thick SiN_x film to increase the capacitance between the two dots. In the following, we denote the two QDs as QD_i ($i = 1,2$), and the side gates as SG_{iL} and SG_{iR} for each sample, as illustrated in Fig. 1(a). We measure the current through QD_i, I_i, at the source–drain bias voltage, V_{SDi}, across the dot, the side-gate voltages, V_{SGiL} and V_{SGiR}, and the back-gate voltage, V_{BG}. All measurements discussed below have been performed in a dilution refrigerator at a base temperature of 20 mK and an electron temperature of 290 mK.

Basic characterization of devices. Figure 1(b) shows the differential conductance of QD_2 in sample A, dI_2/dV_{SD2}, as a function of V_{SD2}, and the side-gate voltage $V_{SG2} = V_{SG2L} = V_{SG2R}$ at $V_{BG} = 0$ V. We observe a series of diamond-shaped Coulomb blockade regions. Some of the diamonds are truncated because of inelastic co-tunnelling processes. Note that the electron numbers in both QD_1 and QD_2 in both samples A and B are not experimentally determined, but we speculate that each of the QDs contains few tens of electrons. From the aspect ratio of the diamonds, we evaluate the lever-arm factor, α, which converts the gate voltage to the change in the electrochemical potential of a QD. We find that α varies with the electron number in the dot, as implied by different aspect ratios of the diamonds in Fig. 1(c). We suppose that α may depend on the spatial distribution

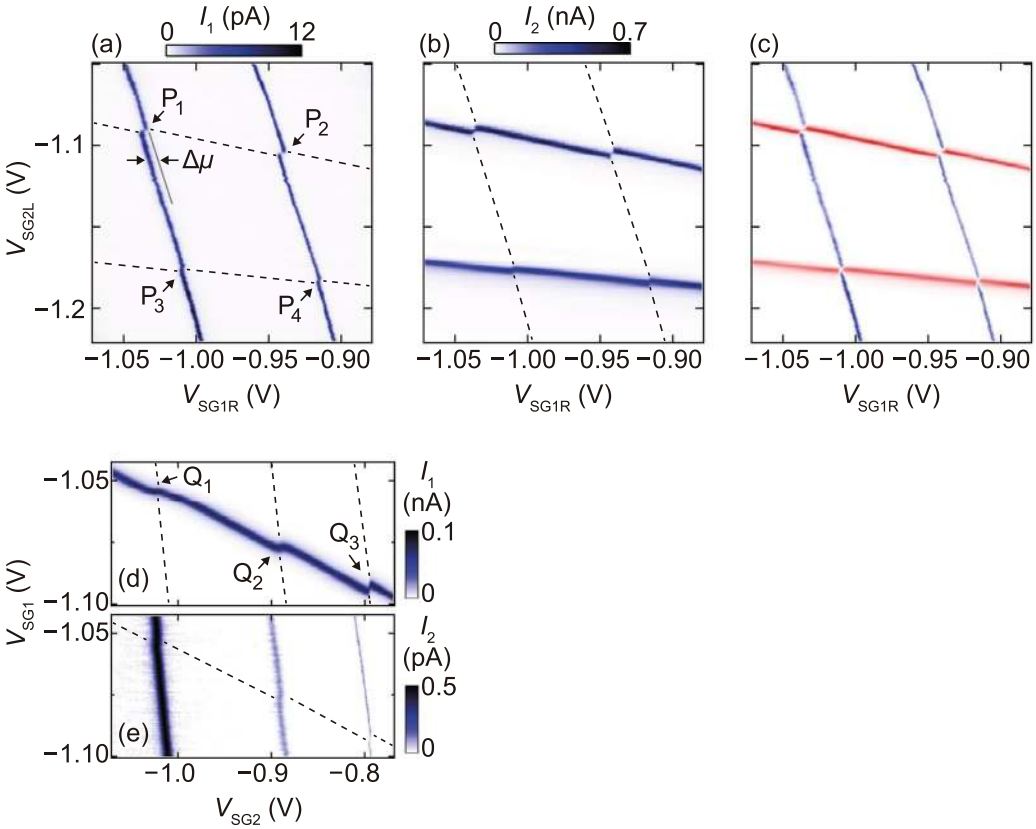

Figure 2. (**a**,**b**) Intensity plots of I_1 (**a**) and I_2 (**b**) in sample A as a function of V_{SG1R} and V_{SG2L} at $V_{BG} = 0$ V and $V_{SD1} = V_{SD2} = 70\,\mu$V. The dashed lines in (**a**) and (**b**) represent the positions of the Coulomb peak ridges in QD_2 and QD_1, respectively. Capacitive coupling between the two QDs and thus charge sensing features are observed at the gate voltage conditions denoted as P_j ($j = 1$–4), where the two ridges in different QDs intersect. (**c**) Superposition plots of (**a**) and (**b**) showing the honeycomb pattern. (**d**,**e**) Intensity plots of I_1 (**d**) and I_2 (**e**) in sample B as a function of V_{SG1} and V_{SG2} at $V_{BG} = 0$ V and $V_{SD1} = V_{SD2} = 70\,\mu$V, showing the charge sensing features at Q_k ($k = 1$–3).

of the wave function in the dot and thus the screening effect, which may change with the electron number. In Fig. 1(c), we show averaged α values of each dot in samples A and B for $V_{SG1} = V_{SG1L} = V_{SG1R}$, V_{SG2} and V_{BG}. Error bars indicate the range of the α values evaluated for single diamonds. For the side gates, the values of α are larger than 40 meV/V, which is an order of magnitude larger than those reported in preceding works[2,3]. These large α values of the side gates are attributed to the gates' locations close to the dots, increased number of side gates, and the reduced screening effect by the narrow source and drain electrodes. The α values of the side gates in samples A are larger than those in sample B, whereas the α values of the back gates are almost the same for both samples. This may indicate the increase in the capacitance between the dot and the side gates by the SiN_x dielectric layer; this is not, however, conclusive because of the electron number dependence of α.

Charge sensing experiments. To investigate the transport properties of one dot in response to single-electron charging in the other, we measure I_1 and I_2 simultaneously. Fig. 2(a,b) show I_1 and I_2, respectively, in sample A as a function of V_{SG1R} and V_{SG2L} at $V_{BG} = 0$ V and $V_{SD1} = V_{SD2} = 70\,\mu$V. We observe two Coulomb peak ridges in each dot in the measured side-gate voltage range. These ridges exhibit a finite slope because each dot has capacitive couplings to both the side gates. Each ridge shows a distinct shift at the gate voltage where the two ridges in the different dots intersect each other. The gate voltage of the ridges shifts towards positive when the electron number in the other dot increases, resulting in a honeycomb pattern [see also Fig. 2(c)] typical of double QDs with an inter-dot capacitive coupling[34]. These features indicate that these shifts of ridges result from the capacitive coupling between the two dots, and thus, the charge sensing of either dot by using the other dot as a sensor is achieved. Note that the inter-dot tunnel coupling is negligibly small. We observed similar charge sensing features in sample B as shown in Fig. 2(d,e).

We evaluate the change in the electrochemical potential of the dot, $\Delta\mu$, induced by single-electron charging in the other dot at the gate voltage conditions P_j ($j = 1$–4) shown in Fig. 2(a) for sample A and Q_k ($k = 1$–3) shown in Fig. 2(d) for sample B. For sample A, $\Delta\mu$ is $220 \pm 20\,\mu$eV at P_1 and P_2, and $110 \pm 20\,\mu$eV at P_3 and P_4. For sample B, $\Delta\mu$ is $110 \pm 20\,\mu$eV at Q_1 and $150 \pm 20\,\mu$eV at Q_2 and Q_3. For each of P_j and Q_k, the values of $\Delta\mu$ evaluated from I_1 [Fig. 2(a,d)] are almost the same as those evaluated from I_2 [Fig. 2(b,e)]. It is difficult to compare $\Delta\mu$ directly between samples A and B because $\Delta\mu$ reflects the details in the wave function geometry in both dots as discussed above for the lever-arm factors in Fig. 1(c). It has been reported that asymmetrically applied side-gate

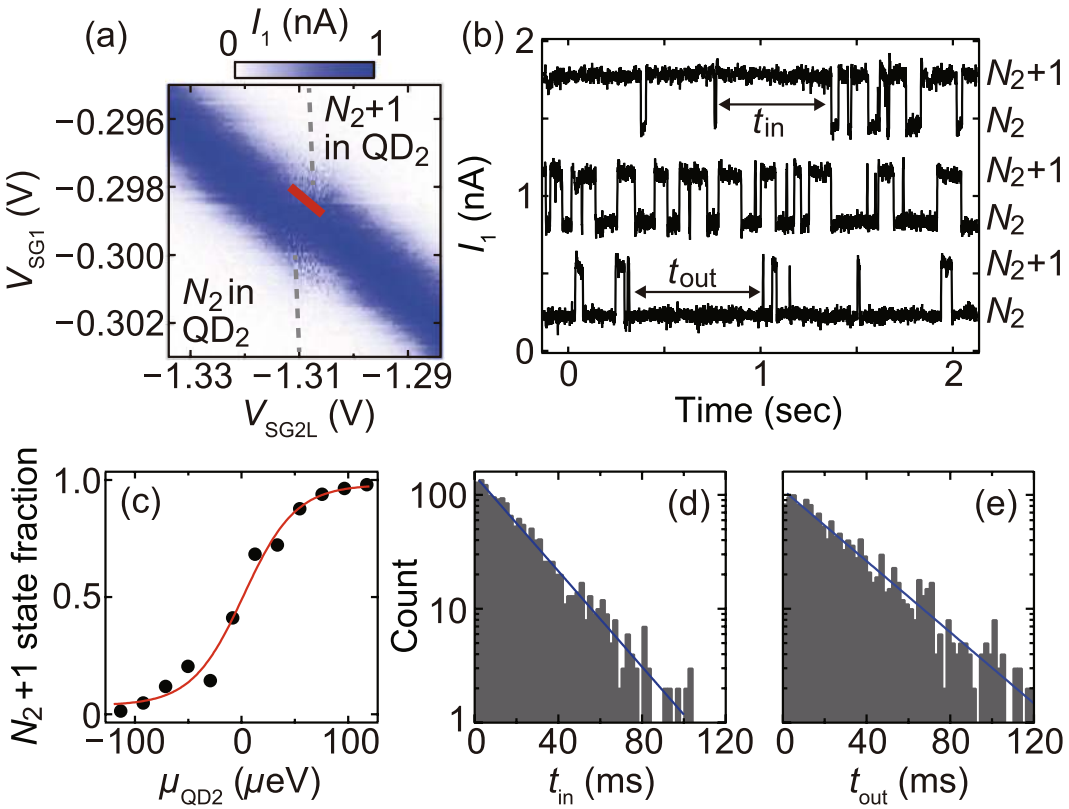

Figure 3. (**a**) Intensity plot of I_1 in sample B as a function of V_{SG1} and V_{SG2L} at $V_{BG} = -0.5$ V, $V_{SD1} = 200\,\mu$V and $V_{SD2} = 0\,\mu$V. (**b**) Real-time traces of I_1 measured at $V_{SG2L} = -1.306$ V (top), -1.309 V (middle), and -1.312 V (bottom) along the red line in (**a**). Each curve is offset by 0.6 nA for clarity. (**c**) $N_2 + 1$ state fraction as a function of μ_{QD2}. A red curve is a fit to the data with the Fermi distribution function. (**d**,**e**) Histograms of t_{in} (**d**) and t_{in} (**e**) obtained at $V_{SG2L} = -1.306$ V, the same condition as the middle I_2 trace in (**b**).

voltage affects the lateral position and the extension of the wave function because of the modulation of the lateral confinement potential of the QDs[4,5]. As seen in Fig. 2(b), for QD_2 in sample A, the electronic state responsible for the lower Coulomb peak ridge couples more strongly to SG_{2L} than the state for the upper ridge. This implies that the orbital wave function in QD_2 is located closer to SG_{2L} and thus farther from QD_1, which is consistent with the smaller $\Delta\mu$ for the lower ridge than the upper one.

Demonstration of real-time charge sensing. We demonstrate the real-time detection of single-electron tunnelling events. Fig. 3(a) shows I_1 in sample B as a function of $V_{SG1} = V_{SG1L} = V_{SG1R}$ and V_{SG2L} for different electron numbers in both QD_1 and QD_2 from Fig. 2(d,e) with $V_{BG} = -0.5$ V, $V_{SD1} = 200\,\mu$V and $V_{SD2} = 0\,\mu$V. We observe the shift in the Coulomb peak ridge for I_1 similar to that observed in Fig. 2(a) to (e), indicating the change in the electron number of QD_2 between N_2 and $N_2 + 1$. The amplitude of I_2 is smaller than the noise floor of approximately 20 fA in the same gate-voltage range, suggesting small tunnel coupling between QD_2 and the leads. We measure I_1 in real-time at the resonance of the charge state transition in QD_2 in Fig. 3(a). For the charge sensing measurements, the gate voltages are set such that the sensor QD_1 is always set on one side of a Coulomb peak. The measurement bandwidth and the sampling frequency are 5 kHz and 2 kHz, respectively. Figure 3(b) shows the real-time traces of I_1 measured at slightly different gate voltage conditions for QD_2 along the red line in Fig. 3(a). We observe distinct random telegraph signals between I_1 values of ~0.2 nA and ~0.5 nA. These low and high I_1 signal levels correspond to the N_2 and $N_2 + 1$ charge states in QD_2, respectively, indicating the detection of single-electron tunnelling events in and out of QD_2. The charge-sensing signal amplitude is ~0.32 nA and the noise amplitude is ~0.08 nA, resulting in the signal-to-noise ratio of ~4. To further confirm the real-time charge sensing, we analyse the gate voltage dependence of the fraction of the N_2 and $N_2 + 1$ charge states. When the electrochemical potential of QD_2, μ_{QD2}, changes with the gate voltages, the fraction of the N_2 and $N_2 + 1$ charge states also changes, reflecting the energy difference between μ_{QD2} and the thermally broadened energy distributions of electrons in the source and drain electrodes. In Fig. 3(b), as V_{SG2L} decreases across the charge state resonance in QD_2 from top to bottom I_1 traces, the fraction of the $N_2 + 1$ state decreases as expected for increasing μ_{QD2}. Figure 3(c) shows the $N_2 + 1$ state fraction as a function of μ_{QD2}. The estimation of the lever-arm factor in this condition is described in Supplementary Information. Numerical fitting using the Fermi distribution function gives an electron temperature of 280 ± 20 mK, which is in good agreement with that estimated from the Coulomb peak width. We define t_{in} and t_{out} for the dot as the lengths of time it resides at the $N_2 + 1$ and N_2 charge states, respectively, and show their histograms in Fig. 3(c,d). Each histogram shows a single exponential distribution.

By fitting them to $\exp(-\Gamma_{in(out)}t_{in(out)})$, where $\Gamma_{in(out)}$ is the rate of electron tunnelling into (out of) the dot, we obtain the tunnel coupling $\gamma = \Gamma_{in} + \Gamma_{out} = 84 \pm 2$ Hz between the dot and the lead. The utility of the real-time charge sensing will be further improved by the ability to independently control the tunnel rate and the charge state in individual QDs. This will be viable by changing voltages on both side and back gates simultaneously so as to modulate the overlap between the lead state and the electronic wave function in the QD while keeping the electrochemical potentials of the QD unchanged[5]. The control of the tunnel rate for arbitrary charge states is to be investigated in our devices in future experiments.

Summary and Prospect. In summary, we have demonstrated charge sensing experiments in InAs self-assembled quantum dots by using one of two adjacent dots as a target and the other as a sensor. We have observed distinct shifts in the Coulomb peak ridges in the sensor dot when the electron number changes by one in the target dot, which is a signature of single-electron charge sensing. We have also demonstrated real-time detection of single-electron tunnelling events, which is an ingredient for the measurement of single spins or single photons. The charge sensing technique presented in this work will be applicable for self-assembled QDs made of other materials, such as GaN[35] and SiGe[36]; this would bring opportunities to investigate intriguing physics of charge and spin in self-assembled QDs. Moreover, the technology can be applicable for self-assembled multiple QD systems[6,37] and QDs coupled to superconductors[5,6] or ferromagnets[7,8], enabling to study the correlated electron spin dynamics. In terms of the applications to photonics, the charge sensing may be realized for single-electron transistors using on optically active QDs having a thin capping layer[38]. Our demonstration of the charge sensing in self-assembled QDs will be an important step towards combining efficient electrical readout of single electron with a variety of transport phenomena and advanced optical and photonic technologies.

Methods

Device fabrication. Uncapped InAs self-assembled QDs are grown by molecular beam epitaxy in the Stranski-Krastanov mode on a semi-insulating (001) GaAs substrate. The growth layers consist of a 300-nm-thick degenerately Si-doped GaAs layer, used as the back gate, followed by a 100-nm-thick $Al_{0.3}Ga_{0.7}As$ barrier layer and a 200-nm-thick undoped GaAs buffer layer. Among the randomly positioned QDs with various sizes, we identify using scanning electron microscope two QDs with size and position suitable for subsequent fabrication. In this work, we choose QDs having diameter and height of approximately 100 nm and 20 nm, respectively, and separated by approximately 150 nm from centre-to-centre. A pair of source and drain electrodes and side-gate electrodes are fabricated on each dot using electron beam lithography and electron beam evaporation of Ti/Au (10/20 nm) [Fig. 1(a)]. Prior to the evaporation, an oxidized layer on the dot surface is removed using *in situ* Ar plasma etching. For sample A, a 50-nm-thick SiN_x film is deposited by the catalytic chemical vapour deposition method.

Measurement details. Measurements are performed in a dilution refrigerator with a base temperature of 20 mK. The measurement lines are filtered with a two-stage RC low-pass filter with a cut-off frequency of 1 MHz. The electron temperature is estimated to be approximately 290 mK from the width of the narrowest Coulomb peaks in our samples.

References

1. Jung, M. *et al*. Shell structures in self-assembled InAs quantum dots probed by lateral electron tunneling structures. *Applied Physics Letters* **87**, 203109 (2005).
2. Kanai, Y. *et al*. Electrically tuned spin-orbit interaction in an InAs self-assembled quantum dot. *Nature Nanotechnology* **6**, 511–516 (2011).
3. Deacon, R. S. *et al*. Electrically tuned g tensor in an InAs self-assembled quantum dot. *Physical Review B* **84**, 041302(R) (2011).
4. Takahashi, S. *et al*. Electrically tunable three-dimensional g-factor anisotropy in single InAs self-assembled quantum dots. *Physical Review B* **87**, 161302(R) (2013).
5. Kanai, Y. *et al*. Electrical control of kondo effect and superconducting transport in a side-gated InAs quantum dot josephson junction. *Physical Review B* **82**, 054512 (2010).
6. Deacon, R. S. *et al*. Cooper pair splitting in parallel quantum dot josephson junctions. *Nature Communications* **6**, 7446 (2015).
7. Hamaya, K. *et al*. Spin transport through a single self-assembled InAs quantum dot with ferromagnetic leads. *Applied Physics Letters* **90**, 053108 (2007).
8. Hamaya, K. *et al*. Electric-field control of tunneling magnetoresistance effect in a Ni/InAs/Ni quantum-dot spin valve. *Applied Physics Letters* **91**, 022107 (2007).
9. Shibata, K., Umeno, A., Cha, K. M. & Hirakawa, K. Photon-assisted tunneling through self-assembled InAs quantum dots in the terahertz frequency range. *Physical Review Letters* **109**, 077401 (2012).
10. Michler, P. *et al*. A quantum dot single-photon turnstile device. *Science* **290**, 2282 (2000).
11. Press, D., Ladd, T. D., Zhang, B. & Yamamoto, Y. Complete quantum control of a single quantum dot spin using ultrafast optical pulses. *Nature* **456**, 218 (2008).
12. De Greve, K. *et al*. Quantum-dot spin-photon entanglement via frequency downconversion to telecom wavelength. *Nature* **491**, 421 (2012).
13. Gao, W., Fallahi, P., Togan, E., Miguel-Sánchez, J. & Imamoglu, A. Observation of entanglement between a quantum dot spin and a single photon. *Nature* **491**, 426 (2012).
14. Schneider, C. *et al*. Lithographic alignment to site-controlled quantum dots for device integration. *Applied Physics Letters* **92**, 183101 (2008).
15. Cha, K. M., Shibata, K. & Hirakawa, K. Single electron transport through site-controlled InAs quantum dots. *Applied Physics Letters* **101**, 223115 (2012).
16. Hanson, R., Kouwenhoven, L. P., Petta, J. R., Tarucha, S. & Vandersypen, L. M. K. Spins in few-electron quantum dots. *Reviews of Modern Physics* **79**, 1217–1265 (2007).
17. Field, M. *et al*. Measurements of coulomb blockade with a noninvasive voltage probe. *Physical Review Letters* **70**, 1311–1314 (1993).
18. Lu, W., Ji, Z., Pfeiffer, L., West, K. & Rimberg, A. Real-time detection of electron tunnelling in a quantum dot. *Nature* **423**, 422–425 (2003).
19. Schleser, R. *et al*. Time-resolved detection of individual electrons in a quantum dot. *Applied Physics Letters* **85**, 2005–2007 (2004).

20. Vandersypen, L. M. K. *et al*. Real-time detection of single-electron tunneling using a quantum point contact. *Applied Physics Letters* **85**, 4394–4396 (2004).
21. Pioda, A. *et al*. Single-shot detection of electrons generated by individual photons in a tunable lateral quantum dot. *Physical Review Letters* **106**, 146804 (2011).
22. Fujita, T. *et al*. Nondestructive real-time measurement of charge and spin dynamics of photoelectrons in a double quantum dot. *Physical Review Letters* **110**, 266803 (2013).
23. Elzerman, J. M. *et al*. Single-shot read-out of an individual electron spin in a quantum dot. *Nature* **430**, 431–435 (2004).
24. Hanson, R. *et al*. Single-shot readout of electron spin states in a quantum dot using spin-dependent tunnel rates. *Physical Review Letters* **94**, 196802 (2005).
25. Barthel, C., Reilly, D. J., Marcus, C. M., Hanson, M. P. & Gossard, A. C. Rapid single-shot measurement of a singlet-triplet qubit. *Physical Review Letters* **103**, 160503 (2009).
26. Kiyama, H., Nakajima, T., Teraoka, S., Oiwa, A. & Tarucha, S. Single-shot ternary readout of two-electron spin states in a quantum dot using spin filtering by quantum hall edge states. *Physical Review Letters* **117**, 236802 (2016).
27. Zaitsu, K., Kitamura, Y., Ono, K. & Tarucha, S. Vertical quantum dot with a vertically coupled charge detector. *Applied Physics Letters* **92**, 033101 (2008).
28. Biercuk, M. J. *et al*. Charge sensing in carbon-nanotube quantum dots on microsecond timescales. *Physical Review B* **73**, 201402(R) (2006).
29. Wallin, D. *et al*. Detection of charge states in nanowire quantum dots using a quantum point contact. *Applied Physics Letters* **90**, 172112 (2007).
30. Shorubalko, I. *et al*. Self-aligned charge read-out for InAs nanowire quantum dots. *Nano Letters* **8**, 382–385 (2008).
31. Vukušić, L., Kukucka, J., Watzinger, H. & Katsaros, G. Fast hole tunneling times in germanium hut wires probed by single-shot reflectometry. *Nano Letters* **17**, 5706–5710 (2017).
32. Shibata, K., Yuan, H., Iwasa, Y. & Hirakawa, K. Large modulation of zero-dimensional electronic states in quantum dots by electric-double-layer gating. *Nature Communications* **4**, 2664 (2013).
33. Shibata, K., Jung, M., Cha, K. M., Sotome, M. & Hirakawa, K. Effect of in-ga intermixing on the electronic states in self-assembled inas quantum dots probed by nanogap electrodes. *Applied Physics Letters* **94**, 162107 (2009).
34. van der Wiel, W. G. *et al*. Electron transport through double quantum dots. *Reviews of Modern Physics* **75**, 1–22 (2002).
35. Nakaoka, T., Kako, S., Arakawa, Y. & Tarucha, S. Coulomb blockade in a self-assembled GaN quantum dot. *Applied Physics Letters* **90**, 162109 (2007).
36. Katsaros, G. *et al*. Hybrid superconductor-semiconductor devices made from self-assembled SiGe nanocrystals on silicon. *Nature Nanotechnology* **5**, 458–464 (2010).
37. Baba, S. *et al*. Superconducting transport in single and parallel double InAs quantum dot josephson junctions with Nb-based superconducting electrodes. *Applied Physics Letters* **107**, 222602 (2015).
38. Nakaoka, T., Watanabe, K., Kumagai, Y. & Arakawa, N. A single-electron probe for buried optically active quantum dot. *AIP advances* **2**, 032103 (2012).

Acknowledgements

We thank S. Baba for help with device fabrication, and T. Hirayama, R. Shikishima for useful discussions. This work was supported by Grant-in-Aid for Young Scientists B (No. 15K17681), Grants-in-Aid for Scientific Research S (No. 17H06120, No. 26220710), Scientific Research A (16H02333), Innovative Areas "Nano Spin Conversion Science" (No. 26103004), Innovative Areas "Science of hybrid quantum systems" (No. 15H05868), Project for Developing Innovation Systems of MEXT, CREST, Japan Science and Technology Agency (JST) (JPMJCR15N2), the Murata Science Foundation, the Asahi Glass foundation, Dynamic Alliance for Open Innovation Bridging Human, Environment and Materials from MEXT, "Nanotechnology Platform Project (Nanotechnology Open Facilities in Osaka University)" of Ministry of Education, Culture, Sports, Science and Technology, Japan (No. F-17-OS-0030, No. S-17-OS-0030), and the PROMOS program of the German Academic Exchange Service.

Author Contributions

H.K. fabricated the devices, performed the measurements, analysed the results and wrote the manuscript. A.K. contributed to the device fabrication and the measurements. N.N. and K.H. grew the uncapped InAs QDs. Y.K. and K.M. deposited the SiN_x layer. A.O. contributed to the interpretation of results and supervised the work. All authors contributed to the discussions and writing of the manuscript.

Additional Information

Supplementary information accompanies this paper at https://doi.org/10.1038/s41598-018-31268-x.

Competing Interests: The authors declare no competing interests.

Publisher's note: Springer Nature remains neutral with regard to jurisdictional claims in published maps and institutional affiliations.